Appl. Phys. A (2014) 117:1467–1472
DOI 10.1007/s00339-014-8576-z

Applied Physics A
Materials Science & Processing

Photoluminescence study of nitrogen-doped p-type $Mg_xZn_{1-x}O$ nanocrystalline thin film grown by plasma-assisted molecular beam epitaxy

Muhammad M. Morshed · Zheng Zuo · Jian Huang · Jian-Guo Zheng · Qiyin Lin · Xiaoqing Yan · Jianlin Liu

Received: 5 April 2014 / Accepted: 16 June 2014 / Published online: 29 June 2014
© Springer-Verlag Berlin Heidelberg 2014

Abstract Temperature-dependent photoluminescence of nitrogen-doped p-type $Mg_xZn_{1-x}O$ nanocrystalline thin film grown on *c*-plane sapphire substrate by rf plasma-assisted molecular beam epitaxy is investigated. P-type behavior is confirmed by both Hall effect and Seebeck measurements. Structural defect-related bound excitonic emission peak is distinguished at around ~50 meV lower than peak energy of the near band edge neutral acceptor bound excitonic emission. Typical 'S shape' behavior of energy position versus temperature is observed due to polarization-induced internal field. Nitrogen-related acceptor ionization energy is calculated to be ~180–200 meV.

1 Introduction

ZnO has attracted much attention for optoelectronic applications such as light emitting diodes (LED) and laser diodes (LD) thanks to its wide band gap of 3.37 eV and high-exciton binding energy (60 meV) at room temperature (RT). $Mg_xZn_{1-x}O$ and $Cd_xZn_{1-x}O$ alloys open up the opportunity for band gap and heterostructure engineering [1, 2]. Extensive research is going on to overcome the bottleneck problem of stable and reproducible p-type ZnO and $Mg_xZn_{1-x}O$. Group-I (Li, Na) and group-V (N, P, Sb, As) elements are mainly introduced as substitutional or defect complex dopants [3–10]. In addition, co-doping or dual doping (N–Ga, Li–N, etc.) is a possible route to successful p-type doping [11, 12].

So far, among all p-type dopants, nitrogen (N) is the most intensively studied candidate [5, 6, 13–17]. Despite some skepticism over the N as successful p-type dopant [18, 19], Tsukazaki et al. [6], Nakahara et el. [20], and Kato et al. [21] demonstrated successful ZnO- and $Mg_xZn_{1-x}O$-based devices using N as p-type dopant. Nakahara et al. [20] and Lautenschlaeger et al. [22] suggested that Zn-polar growth is preferred for increased N_O (N substitutes O) incorporation. Also, Liu et al. [14] reported that N could create a shallow acceptor level by forming a defect complex with zinc vacancy (V_{zn}), $N_O - V_{zn}$.

For successful and reliable p-type N-doping, more evidence of the N as an acceptor is still necessary. Furthermore, although tremendous effort was spent on single-crystalline ZnO-based thin films, study of both n- and p-type doping of ZnO-based micro- and nanocrystalline thin films becomes important because these films have profound impact for various applications such as random lasers [23, 24], thin-film transistors [25], and transparent-conducting oxide [26]. In this work, we investigate the low-temperature photoluminescence (PL) spectra along with electrical and structural features of N-doped p-type $Mg_xZn_{1-x}O$ nanocrystalline thin film.

M. M. Morshed · Z. Zuo · J. Huang · J. Liu (✉)
Department of Electrical Engineering, University of California, Riverside, CA 92521, USA
e-mail: jianlin@ee.ucr.edu

J.-G. Zheng · Q. Lin
The Laboratory for X-ray and Electron Instrumentation (LEXI), California Institute for Telecommunications and Information Technology (Calit2), University of California, Irvine, CA 92697, USA

X. Yan
Nantong College, Jiangsu Open University, Nantong 226006, Jiangsu, People's Republic of China

2 Experiment

N-doped $Mg_xZn_{1-x}O$ thin film was grown on *c*-plane sapphire substrate using rf plasma-assisted molecular beam

epitaxy (MBE). First, sapphire substrate was chemically cleaned in an aqua regia (HNO_3:HCl = 1:3) solution at 150 °C for 20 min, then rinsed in de-ionized water, and finally dried with a nitrogen gun and transferred into the MBE chamber. Elemental Zn (6 N) and Mg (6 N) heated by regular Knudsen effusion cells were used as zinc and magnesium sources. A mixture of oxygen (O_2) and nitrous oxide (N_2O) gas was fed through the radio-frequency plasma generator as the oxygen and nitrogen source. The growth began with a thin buffer layer of MgO and followed by another ZnO buffer at a temperature of 450 °C, with Zn, Mg cell temperatures at 352 and 450 °C, respectively, and 2 sccm of O_2 flow. Subsequently, an $Mg_xZn_{1-x}O$ epitaxial layer was grown at 500 °C with Zn and Mg cells at 348 and 390 °C, respectively, and (2.4:2.6) sccm of O_2:N_2O gas mixture. Then, the sample was in situ annealed at 600 °C for 30 min with 3 sccm of O_2 flow.

A 325-nm He–Cd laser was used as the excitation source to carry out the PL measurements. Absorption spectrum was measured by Varian Cary 500 double beam scanning UV/Vis/NIR spectrophotometer. A home-built heater and heat sink system, together with Kiethley 2401 digital multimeter, were used to measure the thermopower. Room temperature Hall effect measurement was done in a variable magnetic field up to 6,000 gauss. For Hall measurement system, Kiethley 6220 current source and Kiethley 2182 volt meter were used with minimum current capability of 0.1pA with up to 105 V compliance and voltage capability of 1nV, respectively. Au/Ni (100 nm/10 nm) was deposited for 4-contact Hall bar rectangular geometry sample as the contact and also annealed properly using RTA process. Cross-sectional TEM specimen was prepared using focus ion beam in a FEI Quanta 3-D dualbeam system, and TEM image was taken at 200 kV using a Philips CM20 TEM in the LEXI/Calit2 shared-user facility. X-ray diffraction measurement was performed on a Rigaku SmartLab diffractometer at room temperature using Cu Kα radiation and a scintillator detector combined with a diffraction beam monochromator.

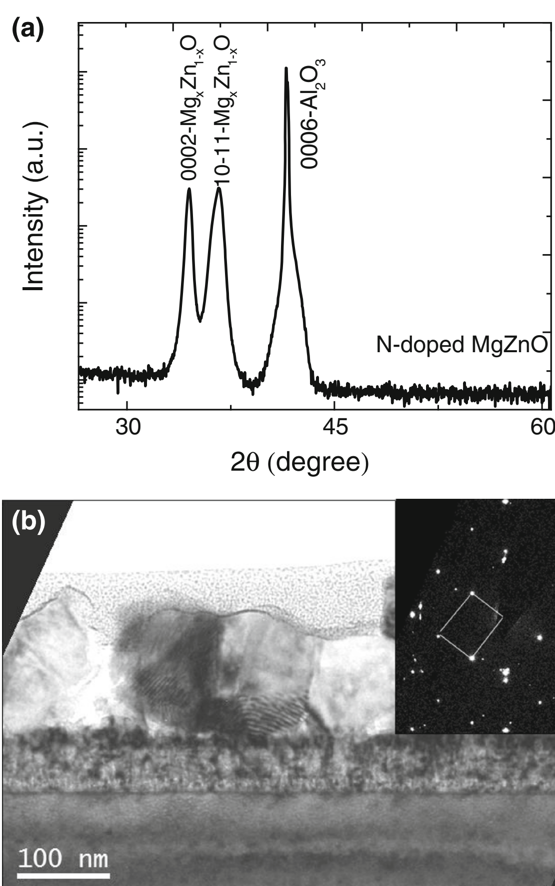

Fig. 1 **a** XRD pattern and **b** bright field cross-sectional TEM image of N-doped $Mg_xZn_{1-x}O$ sample. Top-right inset in **b** is the corresponding SAED pattern, where some of sapphire substrate-related diffraction spots are marked with solid lines to determine the film growth orientation

3 Results and discussion

Figure 1a shows XRD pattern of N-doped $Mg_xZn_{1-x}O$ thin-film sample. This pattern indicates that the N-doped $Mg_xZn_{1-x}O$ thin film has a polycrystalline nature because, besides the 0002 peak, the $10\bar{1}1$ peak of $Mg_{0.15}Zn_{0.85}O$ also shows up at around 36.4° in the pattern. It should be noted that the peak at around 36.4° is broad and contains contribution from the underneath ZnO/MgO buffer layer as well. The conclusions drawn from XRD result are fully supported by TEM data. Figure 1b shows bright field TEM image of the N-doped $Mg_{0.15}Zn_{0.85}O$ thin-film sample. The polycrystalline nature of the N-doped $Mg_{0.15}Zn_{0.85}O$ layer with an average grain size of about 120 nm is evident. High-density dislocations are present in the ZnO/MgO buffer layer. There is no distinct interface between ZnO/MgO layers of about 45 nm due to the intermixing. Besides the diffraction spots from the sapphire substrate indicated by solid lines, the SAED pattern as shown in the inset reveals many $Mg_{0.15}Zn_{0.85}O$-related diffraction spots, which do not have any certain orientation relationship. The polycrystalline nature of the epitaxial film is not only due to the lattice mismatch with the substrate and lower quality ZnO/MgO buffer layer, but also contributed from relatively low growth temperature and oxygen-rich growth ambient, which are favorable conditions for p-type N-doping. Compared with single-crystalline counterparts, nanocrystalline and polycrystalline epitaxial thin films are indispensible for several applications, as claimed earlier.

Figure 2 shows absorption spectrum at RT of the sample. The excitonic resonance peak in the spectrum shows

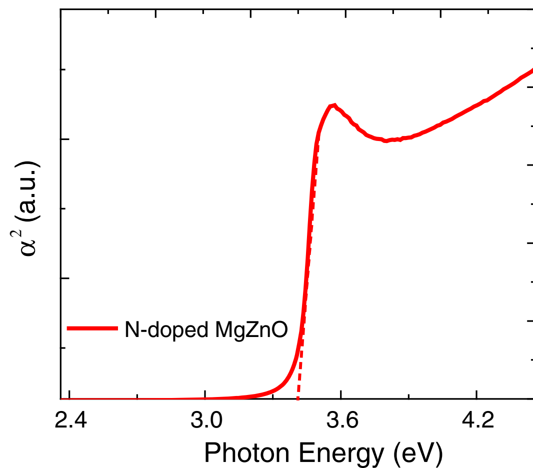

Fig. 2 Square of absorption coefficient (α) at RT of the N-doped $Mg_xZn_{1-x}O$ sample

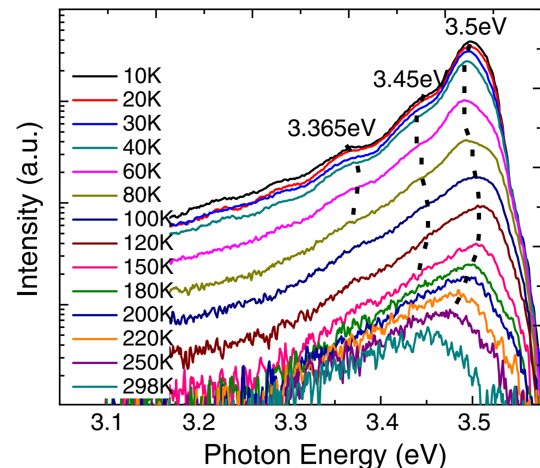

Fig. 4 Temperature-dependent PL spectra of N-doped $Mg_xZn_{1-x}O$ sample

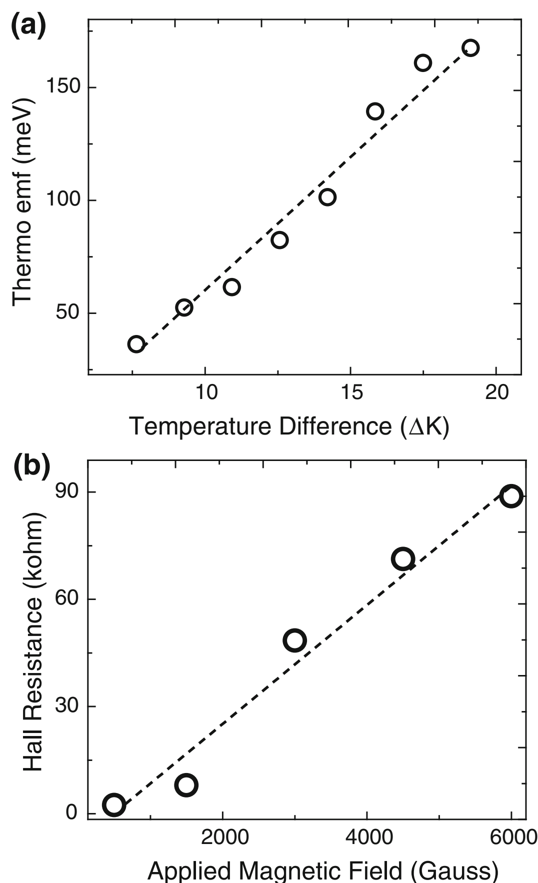

Fig. 3 **a** Variation in thermo e.m.f. with temperature and **b** Hall resistance as a function of the applied magnetic field at RT of N-doped $Mg_xZn_{1-x}O$ sample

good optical quality. Also, the single slope absorption edge ensures no significant phase mixing in the alloy. The absorption edge in the curve indicates an energy band gap of 3.45 eV.

Figure 3a shows Seebeck effect measurement result of the sample. Positive increase in thermopower with the increase in temperature difference is evident, which confirms p-type conductivity. Figure 3b shows RT Hall resistance as a function of magnetic field. Positive increase in Hall resistance with applied magnetic field is observed, further demonstrating p-type conductivity of this sample. The sample exhibits a hole concentration of $3 \times 10^{14} cm^{-3}$ and a resistivity of 240 ohm-cm. The magnitude of the carrier concentration and resistivity should be influenced by the underneath highly conductive buffer layer (multilayer effect) as well as grain boundaries [27, 28]. Moreover, the low carrier concentration could also be due to combined effect of carrier compensation from intrinsic defects and low dopant activation [29, 30].

Figure 4 shows temperature-dependent PL of the sample, from 10 to 298 K. The spectrum at 10 K has three prominent emission peaks. The first peak (Type I) at 3.50 eV should be bound excitonic near band edge (NBE) emission; the second peak (Type II) is separated by 50 meV on the lower energy side (3.45 eV); and the third peak (Type III) is located at 3.365 eV. There have been reports of similarly distributed Type I and Type II emission peaks in ZnO samples, which were mainly attributed to BX (bound exciton)- and FA (free electron to acceptor)-related transitions [5, 16, 31–33]. For example, Reynolds et al. [16] observed an N-related acceptor activation energy of 130 meV and a FA transition at 3.317 eV, which is separated from the BX by ~50 meV in their N-doped ZnO samples. On the other hand, recently, the ~3.31 eV emission was suggested to associate with stacking faults or structural defects in the ZnO crystal [34–36] and assumed to be responsible for p-type behavior [36]. Similar defects-originated peak was reported for GaN and AlGaN, where

the peak is separated by 50–60 meV from the NBE peak [37–40]. As a matter of fact, considering the Type II peak as FA would result in too shallow acceptor ionization energy. Therefore, it is more probable that the Type II peak in our N-doped MgZnO sample is related to structural defects, rather than N-related FA emission.

Considering the p-type conductivity of the sample, the peak at 3.5 eV (Type I) is assigned to neutral acceptor bound excitonic emission (A^0X). There is a shoulder on the higher energy side of the Type I peak, which should be donor bound excitonic emission (D^0X) due to the compensating donors present in the film. Beyond 80 K, the A^0X peak shows blue shift, which is due to thermal dissociation of the acceptor binding energy leading to free excitons.

Figure 5a shows energy positions of the three peaks (Type I–II–III) at different temperature. The Type I peak shows little redshift up to 80 K, which could be due to strain-induced internal polarization [41], and beyond 80 K, it starts dissociating from bound (A^0X) to free exciton (FX). The temperature dependence of FX peak positions can be fitted by Varshni equation [42]

$$E_g(T) = E_g(0) - \frac{\alpha T^2}{T+\beta} \quad (1)$$

and Bose–Einstein (B–E) band gap equation [43, 44]

$$E_g(T) = E_g(0) - \frac{k}{\exp\left(\theta/T\right) - 1} \quad (2)$$

where $E_g(0)$ is the energy position at 0 K, and α, β, (proportional to Debye temperature, θ_D), k, and (Einstein temperature, θ_E) are fitting parameters. Figure 5a also shows the fitting curves (Varshni-orange dash-dotted line and B–E pink dashed line). The parameters used for the Varshni fitting are, $E_{FX}(0) = 3.5157$ eV, $\alpha = 8.5 \times 10^{-4}$ eV/K, $\beta = (1{,}050 \pm 30)$ K and for the B–E fitting are $E_{FX}(0) = 3.5157$ eV, $k = 0.092$ eV and $\theta = (300 \pm 5)$ K. The ratio of θ/β ($\approx \theta_E/\theta_D$) is close to 0.3, which is in good agreement with the value found for ZnO [45] and AlGaN [46]. The Type II peak shows 'S-shaped' temperature dependence. It redshifts up to 80 K, then blueshifts till 120 K, and eventually redshifts due to band gap shrinkage with further increase in temperature. This behavior has also been observed in GaN alloys, which is attributed to alloy potential fluctuation leading to localized excitons [39, 47–49]. The Type III emission peak blueshifts up to 40 K, and subsequently redshifts. This behavior is typical for donor–acceptor pair (DAP) transitions [32]. At higher temperature, the ionization of the donors turns DAP transitions to FA transitions. We can estimate the acceptor activation energy (E_A) from the following DAP-related emission energy expression,

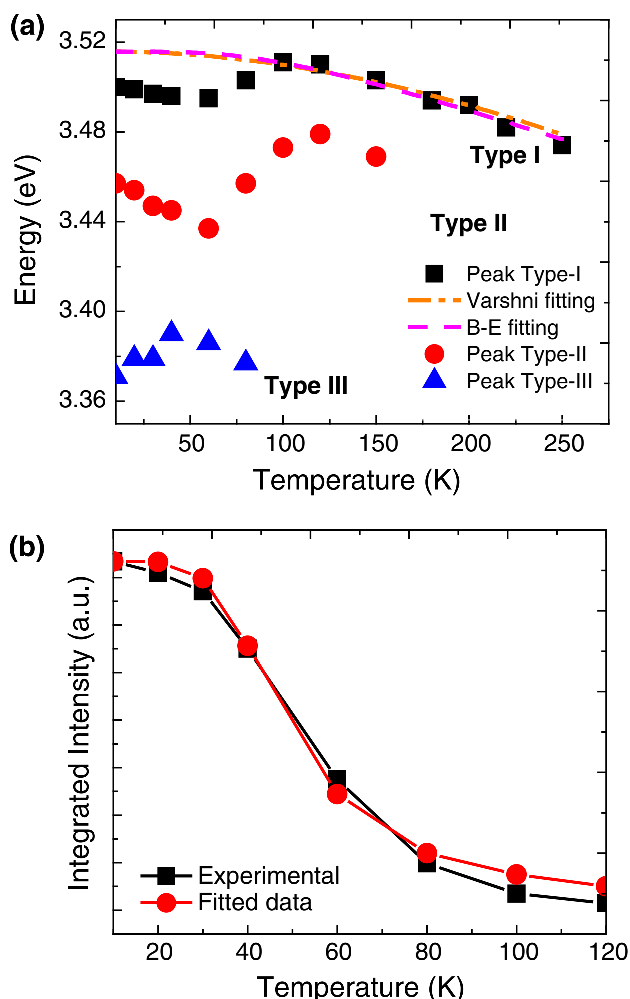

Fig. 5 **a** Energy positions of the PL peaks as a function of temperature of N-doped $Mg_xZn_{1-x}O$ sample. **b** Integrated intensity of the A^0X emission as a function of temperature of N-doped $Mg_xZn_{1-x}O$ sample

$$E_{DAP}(T) = E_g(T) - E_D - E_A + e^2/4\pi\epsilon r_{DA} \quad (3)$$

where, the band gap $E_g = 3.575$ eV, the donor activation energy E_D is estimated to be 40 meV [50], r is the pair separation, which can be estimated by $(3/4\pi N_A)^{1/3}$; ε is the dielectric constant of ZnO (8.6). From equation (3), E_A is calculated to be $\sim$180 meV, where N_A is assumed to be $\sim 10^{15}$ cm^{-3} by considering carrier compensation and multilayer effect [27–29]. This is in good agreement with the results ($E_A \sim$ 170–200 meV) reported by Look et al. and others [5, 51, 52], where N at O site (N_O) was assumed to be the origin, although it is now believed to be from N-related defect complex [14].

Figure 5b shows integrated intensity of the A^0X emission as a function of temperature. The temperature dependence of the integrated PL intensity is given by [53],

$$I(T) = I_0/[1 + C\exp(-E_b^{A^0X}/kT)] \quad (4)$$

where C is a fitting parameter, I_0 is the integrated PL intensity at zero temperature, which is approximately the same as the intensity at $T = 10$ K, and $E_b^{A^0X}$ is the binding energy between the acceptor and free exciton. From the fitting to Eq. (4), $E_b^{A^0X} = 19.1$ meV is obtained. Using the Haynes factor of 0.094 for N-doped ZnO material system [31, 54], the acceptor binding energy E_A is estimated to be 203 meV. This result is in close agreement with the value for the acceptor level obtained using Eq. (3).

4 Conclusion

PL of N-doped p-type $Mg_xZn_{1-x}O$ nanocrystalline thin film is investigated. Structural defect-related emission is distinguished from the N-related emission in the low-temperature PL spectra. Typical 'S shape' behavior of the emission energy position in temperature-dependent PL is observed due to polarization-induced internal field. The ionization energy of N-related acceptor is found to be ~180–200 meV.

Acknowledgments The authors acknowledge the financial support from the Department of Energy (DE-FG02-08ER-46520). FIB and TEM work was performed at the Laboratory for Electron and X-ray Instrumentation (LEXI) at UC Irvine, using instrumentation funded in part by the National Science Foundation Center for Chemistry at the Space–Time Limit (CHE-082913). Web-EMAPS [55] was used to simulate selected area electron diffraction patterns.

References

1. T. Makino, Y. Segawa, M. Kawasaki, A. Ohtomo, R. Shiroki, K. Tamura, T. Yasuda, H. Koinuma, Appl. Phys. Lett. **78**, 1237 (2001)
2. T. Takagi, H. Tanaka, S. Fujita, S. Fujita, Jpn. J. Appl. Phys. **42**, L401 (2003)
3. E. Lee, K.J. Chang, Phys. Rev. B **70**, 115210 (2004)
4. S.S. Lin, Appl. Phys. Lett. **101**, 122109 (2012)
5. D.C. Look, D.C. Reynolds, C.W. Litton, R.L. Jones, D.B. Eason, G. Cantwell, Appl. Phys. Lett. **81**, 1830 (2002)
6. A. Tsukazaki, A. Ohtomo, T. Onuma, M. Ohtani, T. Makino, M. Sumiya, K. Ohtani, S.F. Chichibu, S. Fuke, Y. Segawa, H. Ohno, H. Koinuma, M. Kawasaki, Nature Mater. **4**, 42 (2005)
7. F.X. Xiu, Z. Yang, L.J. Mandalapu, J.L. Liu, Appl. Phys. Lett. **88**, 152116 (2006)
8. S. Limpijumnong, S.B. Zhang, S. Wei, C.H. Park, Phys. Rev. Lett. **92**, 155504 (2004)
9. F.X. Xiu, Z. Yang, L.J. Mandalapu, D.T. Zhao, J.L. Liu, W.P. Beyermann, Appl. Phys. Lett. **87**, 152101 (2005)
10. H.S. Kang, G.H. Kim, D.L. Kim, H.W. Chang, B.D. Ahn, S.Y. Lee, Appl. Phys. Lett. **89**, 181103 (2006)
11. M. Joseph, H. Tabata, T. Kawai, Jpn. J. Appl. Phys. **38**, L1205 (1999)
12. B.Y. Zhang, B. Yao, Y.F. Li, Z.Z. Zhang, B.H. Li, C.X. Shan, D.X. Zhao, D.Z. Shen, Appl. Phys. Lett. **97**, 222101 (2010)
13. T.M. Barnes, K. Olson, C.A. Wolden, Appl. Phys. Lett. **86**, 112112 (2005)
14. L. Liu, J. Xu, D. Wang, M. Jiang, S. Wang, B. Li, Z. Zhang, D. Zhao, C. Shan, B. Yao, D.Z. Shen, Phys. Rev. Lett. **108**, 215501 (2012)
15. W.Z. Xu, Z.Z. Ye, Y.J. Zeng, L.P. Zhu, B.H. Zhao, L. Jiang, J.G. Lu, H.P. He, S.B. Zhang, Appl. Phys. Lett. **88**, 173506 (2006)
16. J.G. Reynolds, C.L. Reynolds Jr, A. Mohanta, J.F. Muth, J.E. Rowe, H.O. Everitt, D.E. Aspnes, Appl. Phys. Lett. **102**, 152114 (2013)
17. K. Nakahara, S. Akasaka, H. Yuji, K. Tamura, T. Fujii, Y. Nishimoto, D. Takamizu, A. Sasaki, T. Tanabe, H. Takasu, H. Amaike, T. Onuma, S.F. Chichibu, A. Tsukazaki, A. Ohtomo, M. Kawasaki, Appl. Phys. Lett. **97**, 013501 (2010)
18. M.C. Tarun, M.Z. Iqbal, M.D. McCluskey, AIP Advances **1**, 022105 (2011)
19. J.L. Lyons, A. Janotti, C.G. Van de Walle, Appl. Phys. Lett. **95**, 252105 (2009)
20. H. Kato, T. Yamamuro, A. Ogawa, C. Kyotani, M. Sano, Appl. Phys. Express **4**, 091105 (2011)
21. S. Lautenschlaeger, S. Eisermann, B.K. Meyer, G. Callison, M.R. Wagner, A. Hoffmann, Phys. Status Solidi RRL **3**, 16 (2009)
22. J. Huang, S. Chu, J. Kong, L. Zhang, C.M. Schwarz, G. Wang, L. Chernyak, Z. Chen, J. Liu, Adv. Opt. Mater. **1**, 179 (2013)
23. Z.K. Tang, G.K.L. Wong, P. Yu, M. Kawasaki, A. Ohtomo, H. Koinuma, Y. Segawa, Appl. Phys. Lett. **72**, 3270 (1998)
24. S. Chu, M. Olmedo, Z. Yang, J. Kong, J. Liu, Appl. Phys. Lett. **93**, 181106 (2008)
25. B. Bayraktaroglu, K. Leedy, R. Neidhard, IEEE Electron Dev. Lett. **29**, 1024 (2008)
26. X. Jiang, F.L. Wong, M.K. Fung, S.T. Lee, Appl. Phys. Lett. **83**, 1875 (2003)
27. D.C. Look, J. Appl. Phys. **104**, 063718 (2008)
28. D.C. Look, H.L. Mosbacker, Y.M. Strzhemechny, L.J. Brillson, Superlattices Microstruct. **38**, 406 (2005)
29. E. Lee, Y.S. Kim, Y.G. Jin, K.J. Chang, Phys. Rev. B **64**, 085120 (2001)
30. V. Avrutin, D.J. Silversmith, H. Morkoc, Proc. IEEE **98**, 1269 (2010)
31. K. Tang, S. Gu, J. Ye, S. Huang, R. Gu, R. Zhang, Y. Zheng, J. Appl. Phys. **112**, 103534 (2012)
32. J.W. Sun, Y.M. Lua, Y.C. Liub, D.Z. Shen, Z.Z. Zhang, B. Yao, B.H. Li, J.Y. Zhang, D.X. Zhao, X.W. Fan, J. Appl. Phys. **102**, 043522 (2007)
33. X. Meng, Z. Shi, X. Chen, X. Zeng, Z. Fu, X.D. Meng, Z.M. Shi, X.B. Chen, X.H. Zeng, Z.X. Fu, J. Appl. Phys. **107**, 023501 (2010)
34. W. Lin, U. Jahn, H.T. Grahn, L. Chang, M.M.C. Chou, J. Wu, Appl. Phys. Express **6**, 061101 (2013)
35. S. Yang, C.C. Kuo, W. Liu, B.H. Lin, H. Hsu, C. Hsu, W.F. Hsieh, Appl. Phys. Lett. **100**, 101907 (2012)
36. M. Schirra, R. Schneider, A. Reiser, G.M. Prinz, M. Feneberg, J. Biskupek, U. Kaiser, C.E. Krill, K. Thonke, R. Sauer, Phys. Rev. B **77**, 125215 (2008)
37. S. Fischer, G. Steude, D.M. Hofmann, F. Kurth, F. Anders, M. Topf, B.K. Meyer, F. Bertram, M. Schmidt, J. Christen, L. Eckey, J. Holst, A. Homann, B. Mensching, B. Rauschenbach, J. of Crystal Growth **189**, 556 (1998)
38. R. Liu, A. Bell, F.A. Ponce, C.Q. Chen, J.W. Yang, M.A. Khan, Appl. Phys. Lett. **86**, 021908 (2005)
39. P. Corfdir, P. Lefebvre, J. Levrat, A. Dussaigne, J. Ganière, D. Martin, J. Ristić, T. Zhu, N. Grandjean, B. Deveaud-Plédran, J. Appl. Phys. **105**, 043102 (2009)
40. H. Huang, Y. Wu, T. Lu, J. Electrochemical Soc. **158**, H491 (2011)
41. T. Makino, T. Yasuda, Y. Segawa, A. Ohtomo, K. Tamura, M. Kawasaki, H. Koinuma, Appl. Phys. Lett. **79**, 1282 (2001)
42. Y.P. Varshni, Physica **34**, 149 (1967)

43. L. Vin, S. Logothetidis, M. Cardona, Phys. Rev. B **30**, 1979 (1984)
44. S. Logothetidis, L. Vin, M. Cardona, Phys. Rev. B **31**, 947 (1985)
45. L. Wang, N.C. Gilesa, J. Appl. Phys. **94**, 973 (2003)
46. D. Brunner, H. Angerer, E. Bustarret, F. Freudenberg, R. Hopler, R. Dimitrov, O. Ambacher, M. Stutzmann, J. Appl. Phys. **82**, 5090 (1997)
47. Y. Cho, G.H. Gainer, A.J. Fischer, J.J. Song, S. Keller, U.K. Mishra, S.P. DenBaars, Appl. Phys. Lett. **73**, 3689 (1998)
48. Q. Li, S.J. Xu, W.C. Cheng, M.H. Xie, S.Y. Tong, C.M. Che, H. Yang, Appl. Phys. Lett. **79**, 1810 (2001)
49. K.B. Lee, P.J. Parbrook, T. Wang, F. Ranalli, T. Martin, R.S. Balmer, D.J. Wallis, J. Appl. Phys. **101**, 053513 (2007)
50. K. Thonke, T. Gruber, N. Teofilov, R. Schonfelder, A. Waag, R. Sauer, Phys. B **308**, 945 (2001)
51. D.C. Look, Semicond. Sci. Technol. **20**, S55 (2005)
52. L. Wang, N.C. Giles, Appl. Phys. Lett. **84**, 3049 (2004)
53. M. Leroux, N. Grandjean, B. Beaumont, G. Nataf, F. Semond, J. Massies, P. Gibart, J. Appl. Phys. **86**, 3721 (1999)
54. J.G. Lu, Q.N. Liang, Y.Z. Zhang, Z.Z. Ye, S.Z. Fujita, J. Phys. D Appl. Phys. **40**, 3177 (2007)
55. J.M. Zuo, J.C. Mabon, Web-based electron microscopy application software: web-EMAPS. Microsc. Microanal. **10**(Suppl 2), 1000 (2004)